Laser and Particle Beams

cambridge.org/lpb

Collimated proton beams from magnetized near-critical plasmas

Deep Kumar Kuri[1], Nilakshi Das[1] and Kartik Patel[2]

[1]Department of Physics, Tezpur University, Tezpur, Assam-784028, India and [2]UM-DAE Centre for Excellence in Basic Sciences, Mumbai-400098, India

Research Article

Cite this article: Kuri DK, Das N, Patel K (2018). Collimated proton beams from magnetized near-critical plasmas. *Laser and Particle Beams* **36**, 276–285. https://doi.org/10.1017/S0263034618000307

Received: 21 April 2018
Accepted: 23 July 2018

Key words:
3D-PIC simulation; collimated proton beams; magnetic field; near-critical plasmas

Author for correspondence:
Deep Kumar Kuri, Department of Physics, Tezpur University, Tezpur, Assam-784028, India. E-mail: deepkuri303@gmail.com

Abstract

Generation of collimated proton beams by linearly and circularly polarized (CP) lasers from magnetized near-critical plasmas has been investigated with the help of three-dimensional (3D) particle-in-cell (PIC) simulations. Due to cyclotron effects, the transverse proton momentum gets significantly reduced in the presence of an axial magnetic field which leads to an enhancement in collimation. Collimation is observed to be highest in case of a linearly polarized (LP) laser in the presence of magnetic field. However, protons accelerated by a right CP laser in the presence of magnetic field are not only highly collimated but are also more energetic than those accelerated by the LP laser. Although, the presence of an axial magnetic field enhances the collimation by reducing the transverse proton momentum, the maximum proton energy gets reduced since the transverse proton momentum has a significant contribution towards proton energy.

Introduction

With the advent of high-power lasers, generation of high energetic ions has become possible by the interaction of high-intensity laser pulses with plasmas. Ion acceleration has become an interesting and active area of research due to its numerous applications such as fast ignition scenarios (Roth *et al*., 2001), proton radiography (King *et al*., 1999), proton imaging techniques (Borghesi *et al*., 2003), nuclear physics (Bychenkov *et al*., 1999), cancer therapy (Khoroshkov and Minakova, 1998; Bulanov *et al*., 2002), as well as in astrophysics (Remington *et al*., 2000). Multi-MeV ions generated experimentally (Clark *et al*., 2000; Maksimchuk *et al*., 2000; Snavely *et al*., 2000; Fuchs *et al*., 2006) can be explained *via* The target normal sheath acceleration (TNSA) (Wilks *et al*., 2001; Mora, 2003) mechanism in which the ions are accelerated from the target rear side by a sheath field generated by a cloud of hot electrons. The hot electrons generated by the high-intensity laser at the target front-side travel through the target and on reaching the target rear side form a highly negatively charged sheath whose electric field accelerates the ions in the target normal direction. Ions can be accelerated more effectively by the laser ponderomotive force to high energies from the target front side by using ultra intense circularly polarized (CP) laser pulses *via* radiation pressure acceleration (RPA) (Naumova *et al*., 2009; Schlegel *et al*., 2009).

Most of the ion acceleration experiments deal with solid target interactions. Near-critical plasmas such as cluster gas targets and foam targets can also be used to accelerate ions efficiently up to multi-MeV energies and also to enhance the collimation of energetic ion beam. Collimation is a very essential characteristic of accelerated ions which should be enhanced as the lack of collimation limits the use of high energetic ions for potential applications. Replenishable cluster targets facilitate high repetition rate of accelerated ions which are free from plasma debris and are highly collimated (Fukuda *et al*., 2009). The motion of a laser pulse through near-critical plasma targets can lead to the formation of magnetic dipole structure which can accelerate the ions efficiently from the target rear side *via* magnetic vortex acceleration (MVA) (Bulanov and Esirkepov, 2007; Fukuda *et al*., 2009; Bulanov *et al*., 2010; Nakamura *et al*., 2010a) generating collimated energetic ions. Moreover, near-critical targets support the formation of plasma waveguide which makes it possible for the laser pulse to penetrate deeper into the plasma and generate abundant number of hot electrons. Nakamura *et al*. (2010b) have reported experimental results on ion acceleration from SiO_2 foam attached with a thin Al target. They have observed that the bulk electrons inside the foam region are heated up to MeV energies and abundant number of hot electrons are generated which increases the laser–plasma energy coupling and enhances the maximum ion energy. Bin *et al*. (2015) have reported experimental results supported by three-dimensional (3D) particle-in-cell (PIC) simulations on accelerating ions from carbon nanotube foams attached with thin diamond-like carbon targets. They have observed that the high-intensity laser pulse on propagating through the near-critical carbon nanotube region undergoes relativistic self-focussing resulting in an extremely steep rising edge laser pulse profile which causes a significant

CAMBRIDGE UNIVERSITY PRESS

enhancement in the carbon ion energies consistent with a transition to RPA. Willingale *et al.* (2006) have reported an experimental observation of a collimated He^{2+} ion beam generated *via* TNSA mechanism having a maximum energy of 40 MeV by a petawatt-class laser from a gas jet target. Ions can also be accelerated to multi-MeV energies from underdense plasmas (Krushelnick *et al.*, 1999). A very high-intensity laser on propagation through the underdense plasma causes a ponderomotive expulsion of electrons from the high-intensity region at the central axis along the radial directions which create a central ion channel. Thus, a large space-charge field is generated which accelerates the ions along transverse directions *via* Coulomb explosion (Sarkisov *et al.*, 1999). Ions can also be accelerated from underdense plasmas *via* collisionless shock acceleration (Wei *et al.*, 2004). However, these accelerated ions have poor collimation due to high transverse momentum. Willingale *et al.* (2009) have reported experimental observations on the propagation of a high-intensity laser in foam targets generating energetic proton beams in the relativistic transparent regime. They have observed that the laser beam propagates deeper into the target due to its relativistic propagation and results in greater collimation of the hot electrons which enhances the rear surface accelerating field and hence increases the efficiency of acceleration.

Generation of ultra-strong magnetic fields has gained a lot of interest recently. Magnetic fields of the order of 100 T sustainable up to longer time duration can now be readily produced using conventional techniques (Sims *et al.*, 2008; Debray and Frings, 2013). Higher strength fields operating at shorter timescales are also produced (Schmit *et al.*, 2014). Interaction of intense ultrashort laser pulses with dense plasmas can lead to the generation of huge magnetic fields of the order of 10^8 G (Wilks *et al.*, 1992; Sandhu *et al.*, 2002; Tatarakis *et al.*, 2002; Mondal *et al.*, 2012). Magnetic fields of the order of kT can be produced experimentally in the interaction of kilo-Joule high-power lasers with a capacitor-coil target (Fujioka *et al.*, 2013; Santos *et al.*, 2015) which is significant for a number of applications such as inertial confinement fusion (Wang *et al.*, 2015). These magnetic fields can play a significant role in the high-energy electron flow induced during intense laser–plasma interactions and hence has attracted the attention of a lot of researchers working in this field. Hosokai *et al.* (2006) have experimentally observed that the emittance and total charge of electron beams generated by laser-wakefield acceleration gets significantly enhanced on applying a static magnetic field directed along the laser axis of propagation. The formation of solitons during the interaction of an intense laser pulse with plasma in the presence of a strong magnetic field has been studied (Farina *et al.*, 2000; Borhanian *et al.*, 2009). Bulanov *et al.* (2013) have presented an analytical description of the strongly non-linear oscillations in magnetized plasmas, which show that the magnetic field prevents the closing of the cavity formed behind the laser pulse. Yang *et al.* (2015) have shown that the plasma transparency in the presence of magnetic field gets enhanced in case of a right circularly polarized (RCP) light, which is beneficial for plasma acceleration. Wilson *et al.* (2017) have presented an analytical description as well as 1D and 3D-PIC simulation results on the influence of externally applied strong magnetic fields on laser pulse propagation in an underdense plasma and have shown that the electron motion gets dramatically enhanced in case of an RCP light, whereas in case of a left circularly polarized (LCP) light, the electron motion gets dampened and causes a reduction in instability growth. Sharma *et al.* (2010) have analytically investigated the acceleration of ions from an overdense plasma target and have shown that RCP and LCP lasers act differently towards acceleration due to a change in dielectric constant because of cyclotron effects which in turn enhance or reduce the ponderomotive force. Kuri *et al.* (2017) have presented 3D-PIC simulation results where they have shown that the axial magnetic field favors acceleration by TNSA in case of an RCP laser, whereas protons get accelerated more effectively to higher energy by RPA in case of a LCP laser. Gong *et al.* (2017) have investigated the acceleration of protons by an RCP laser from a cone target in the presence of a 50 000 T longitudinal magnetic field *via* 2D-PIC simulations. They have shown that both the energy and yield of the sheath-accelerated protons at the target rear side increase remarkably due to enhanced coupling efficiency from RCP laser energy to electrons.

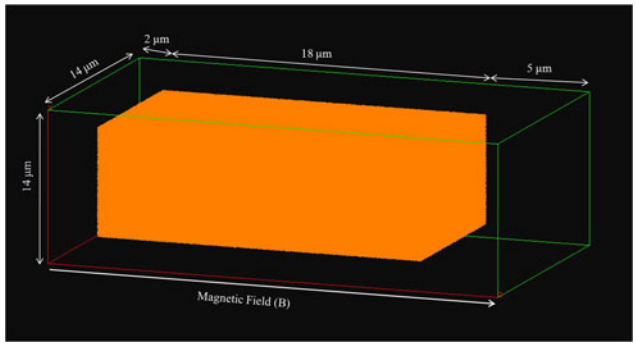

Fig. 1. The 3D-PIC geometry of the simulation box.

In the present work, we investigate the role played by an axial magnetic field in accelerating protons and most importantly in enhancing the collimation of the accelerated protons from a near-critical plasma target by linearly polarized (LP) and CP laser pulses with the help of 3D-PIC simulations using the code Picpsi-3D (Upadhyay *et al.*, 2012). It is observed that the collimation of proton beams increases significantly in the presence of an axial magnetic field. Collimation is observed to be highest in case of a LP laser in the presence of magnetic field. However, protons accelerated by an RCP laser are not only highly collimated but are also highly energetic having highest axial momentum. The paper is organized as follows. "The 3D-PIC simulation model" section represents the detailed parameters of 3D-PIC simulation. Detailed analysis of proton acceleration and beam collimation has been presented in "Generation of collimated proton beams" section. The conclusions are presented in "Conclusion" section.

The 3D-PIC simulation model

A laser of wavelength $\lambda = 1$ μm, normalized electric field amplitude $a_0 (= eE_0/m_e\omega c) \approx 6$ which corresponds to an intensity of 5×10^{19} W/cm^2, pulse duration $\tau = 50$ fs (FWHM) is incident on a near-critical plasma target of density 3.35×10^{21} cm^{-3} ($3n_c$). Here, $n_c = m_e\omega^2/4\pi e^2$ is the critical density, where e and m_e are the charge and mass of an electron, respectively, ω is the laser frequency, E_0 is the laser electric field amplitude, and c is the speed of light. The spot size of the laser pulse is 3 μm (FWHM) and the laser period $T_0 (= \lambda/c)$ is 3.3 fs. A simulation box of dimensions 14 μm × 14 μm × 25 μm consisting of 140 × 140 × 250 cells has been used. The near-critical plasma of height and width 10 μm and thickness 18 μm is sharply edged and is located at a distance of 2 μm from the left boundary of the simulation box as shown in Figure 1. The plasma thickness of

https://doi.org/10.1017/S0263034618000307 Published online by Cambridge University Press

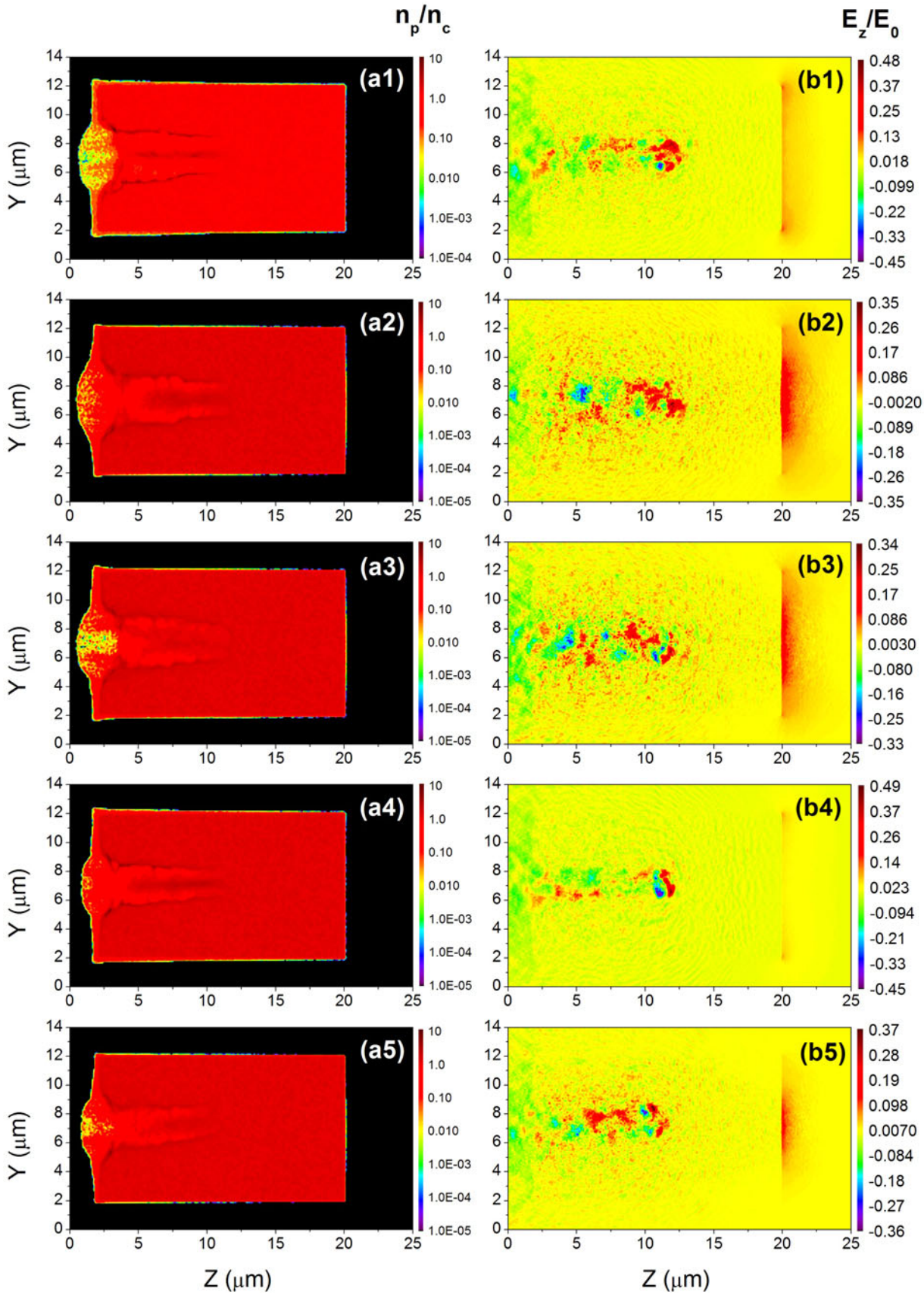

Fig. 2. Proton density distribution (a1–a5) and axial electric field (b1–b5) in the central *YZ* plane ($X = 7$ μm) at time 101 T_0, respectively, for (a1, b1) CP with $B = 0$ G; (a2, b2) RCP with $B = 50$ MG; (a3, b3) LCP with $B = 50$ MG; (a4, b4) LP with $B = 0$ G; and (a5, b5) LP with $B = 50$ MG. The proton density n_p is normalized by the critical density $n_c = 1.12 \times 10^{21}$ cm^{-3} and the axial electric field E_z is normalized by the laser electric field E_0.

https://doi.org/10.1017/S0263034618000307 Published online by Cambridge University Press

18 μm is chosen to ensure complete laser penetration. Since, the length ($=c\tau$) of the laser pulse is 15 μm, the plasma thickness should be at least of the order of laser pulse length in order to achieve maximum penetration. This deep penetration results in volumetric heating of the plasma slab generating large number of hot electrons which can create strong electric fields. A magnetic field of $B = 50$ MG ($\omega_{ce}/\omega \approx 0.5$) is applied along Z which is the axial direction. The simulations have been done for five different cases (i) CP with $B = 0$ G, (ii) RCP with $B = 50$ MG, (iii) LCP with $B = 50$ MG, (iv) LP with $B = 0$ G, and (v) LP with $B = 50$ MG. A vacuum gap of 5 μm is maintained across the target rear side in all cases. Absorbing boundary conditions has been incorporated along all the three directions. The simulations are done with 25 macroparticles per cell. The ions considered in these simulations are protons with mass $m_i = 1836\ m_e$. $\omega_{pe} = \sqrt{4\pi n_e e^2/m_e}$ and $\omega_{ce} = eB/m_e c$ are the electron plasma frequency and electro cyclotron frequency, respectively, where n_e is the electron plasma density. The plasma is initially assumed to be cold with $T_e = T_i = 0$, where T_e and T_i are the electron and ion temperatures, respectively.

Generation of collimated proton beams

The cyclotron effects play an important role in the generation of hot electrons. An RCP laser and a LCP laser act differently on electrons in the presence of an axial magnetic field due to cyclotron effects. In case of an RCP laser, the direction of rotation of electrons by the laser electric field and the direction of electron gyrations by an axial magnetic field are same, which enhances the effect of the laser ponderomotive force. Hence, the electrons gain more energy in case of an RCP laser. On the other hand, in case of a LCP laser, the direction of electron rotations by the laser electric field and the axial magnetic field gyrations is opposite which reverses the cyclotron effects. This opposes the electron motion and causes a reduction in the electron energy. Thus, the electrons move longer distances on gaining higher energy in case of an RCP laser. Whereas, in case of a LCP laser, the electrons tend to get accumulated at the tip of the laser pulse, which may increase the local electron density at the laser pulse front (Kuri *et al.*, 2017).

The hot electrons reach the target rear side and form a hot electron sheath which accelerates the protons from the target rear side *via* TNSA mechanism as shown in Figure 2. Since, the electrons gain more energy by an RCP laser in the presence of an axial magnetic field, the hot electrons reach the target rear side quickly and form the hot electron sheath. The axial sheath electric field is strongest in case of an RCP laser as compared with all the other cases at time 101 T_0 as shown in Figure 2(b2). Comparing Figure 2(b1) and 2(b4), it can be observed that in the absence of magnetic field, the sheath field by a CP laser is stronger than that by a LP laser. This might be due to the dominant effect of radiation pressure as the oscillatory component of the ponderomotive force is absent in case of a CP laser. Since, the transverse motion of the hot electrons generated by a LP laser gets restricted in the presence of an axial magnetic field, the hot electron number as well as the energy along the axial direction is increased which makes the sheath field stronger as shown in Figure 2(b5).

Comparing all the five cases at time 101 T_0, it can be observed that the protons gain highest momentum at the target rear side in case of an RCP laser in the presence of an axial magnetic field due to efficient hot electron generation as shown in Figure 3(b).

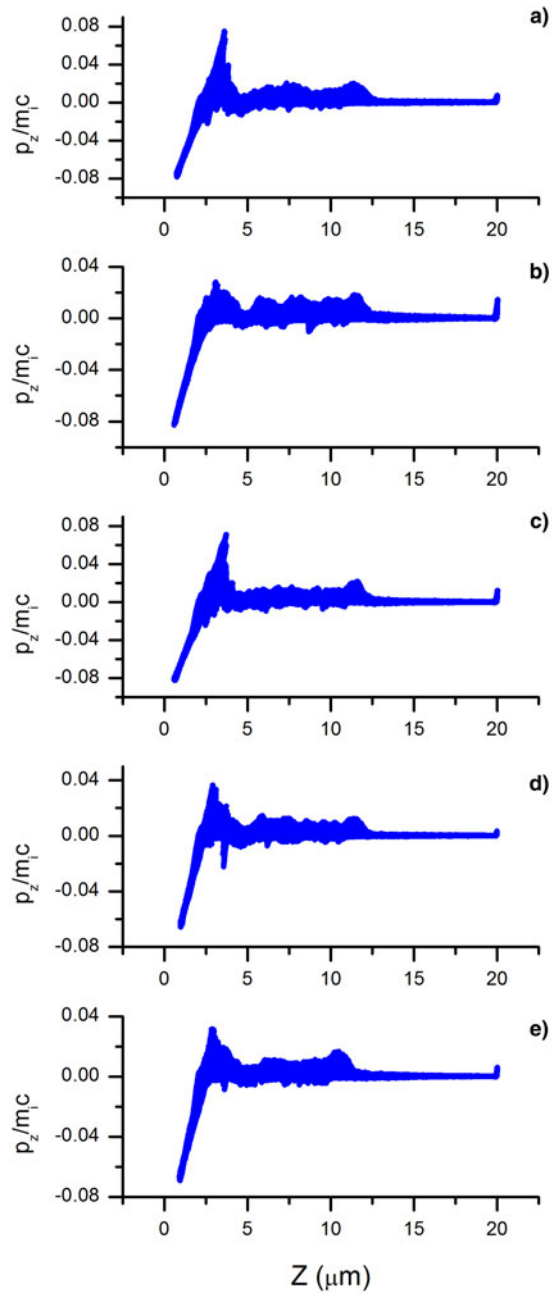

Fig. 3. Normalized proton axial momentum p_z/m_ic phase space for (a) CP with $B = 0$ G, (b) RCP with $B = 50$ MG, (c) LCP with $B = 50$ MG, (d) LP with $B = 0$ G, and (e) LP with $B = 50$ MG at time 101 T_0.

However, it can also be observed that the forward momentum gained by the protons at the target front side is higher in case of a CP laser in the absence of magnetic field and a LCP laser in the presence of magnetic field as shown in Figure 3(a) and 3(c) respectively. Since, the oscillatory component of the laser ponderomotive force is absent in case of a CP laser, the radiation pressure can effectively form an electrostatic charge separation region at the target front side and accelerate protons in the forward direction. In case of a LCP laser, due to reverse cyclotron effects, there might be an electron accumulation at the laser pulse front which can strengthen the electrostatic charge separation region at the target front side and accelerate protons effectively in the forward direction. Thus, traces of RPA-accelerated

https://doi.org/10.1017/S0263034618000307 Published online by Cambridge University Press

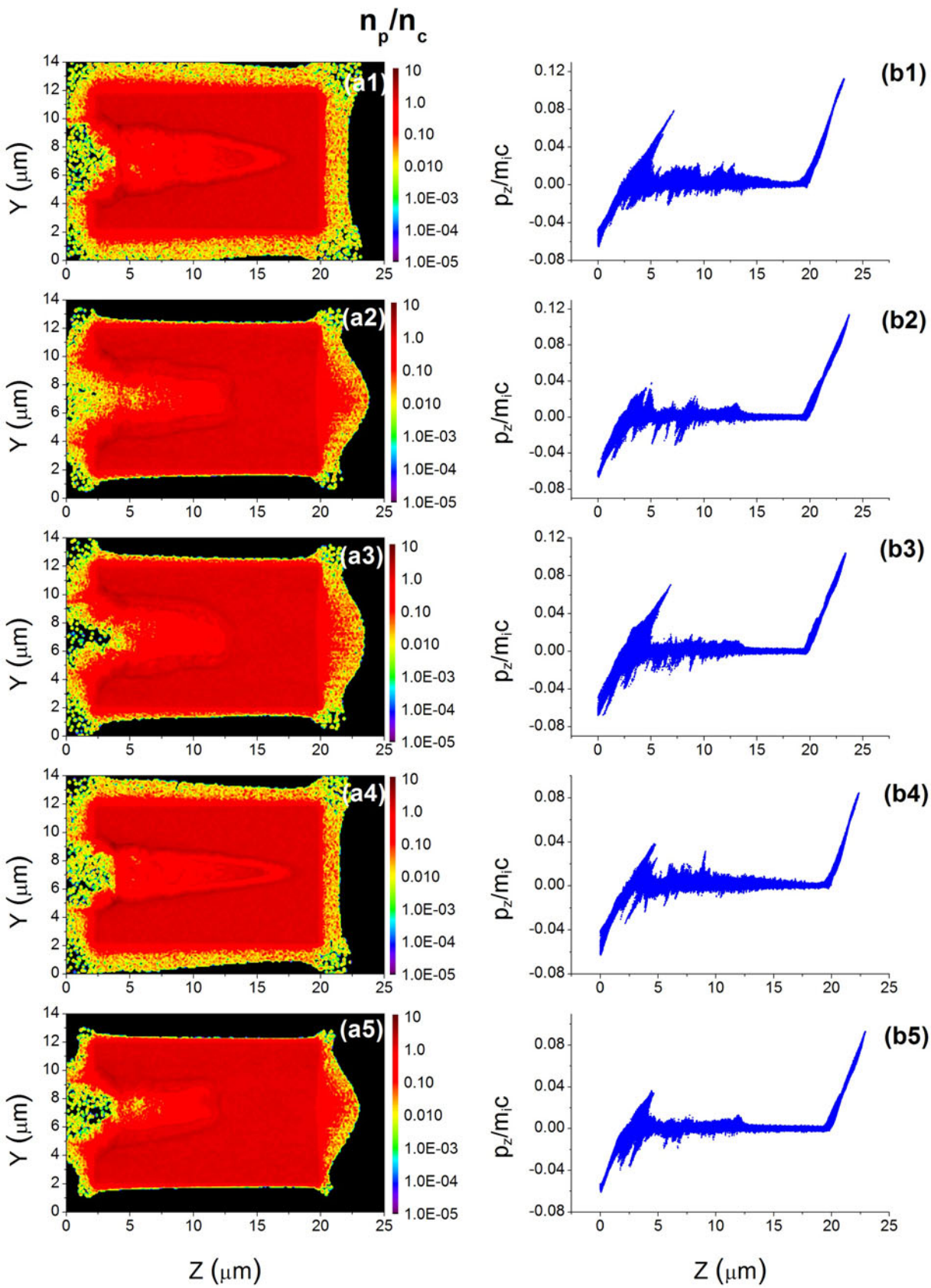

Fig. 4. Proton density distribution (a1–a5) in the central *YZ* plane ($X = 7$ μm) and normalized proton axial momentum p_z/m_ic phase space (b1–b5) at time 147 T_0, respectively, for (a1, b1) CP with $B = 0$ G; (a2, b2) RCP with $B = 50$ MG; (a3, b3) LCP with $B = 50$ MG; (a4, b4) LP with $B = 0$ G; and (a5, b5) LP with $B = 50$ MG. The proton density n_p is normalized by the critical density $n_c = 1.12 \times 10^{21}$ cm^{-3}.

https://doi.org/10.1017/S0263034618000307 Published online by Cambridge University Press

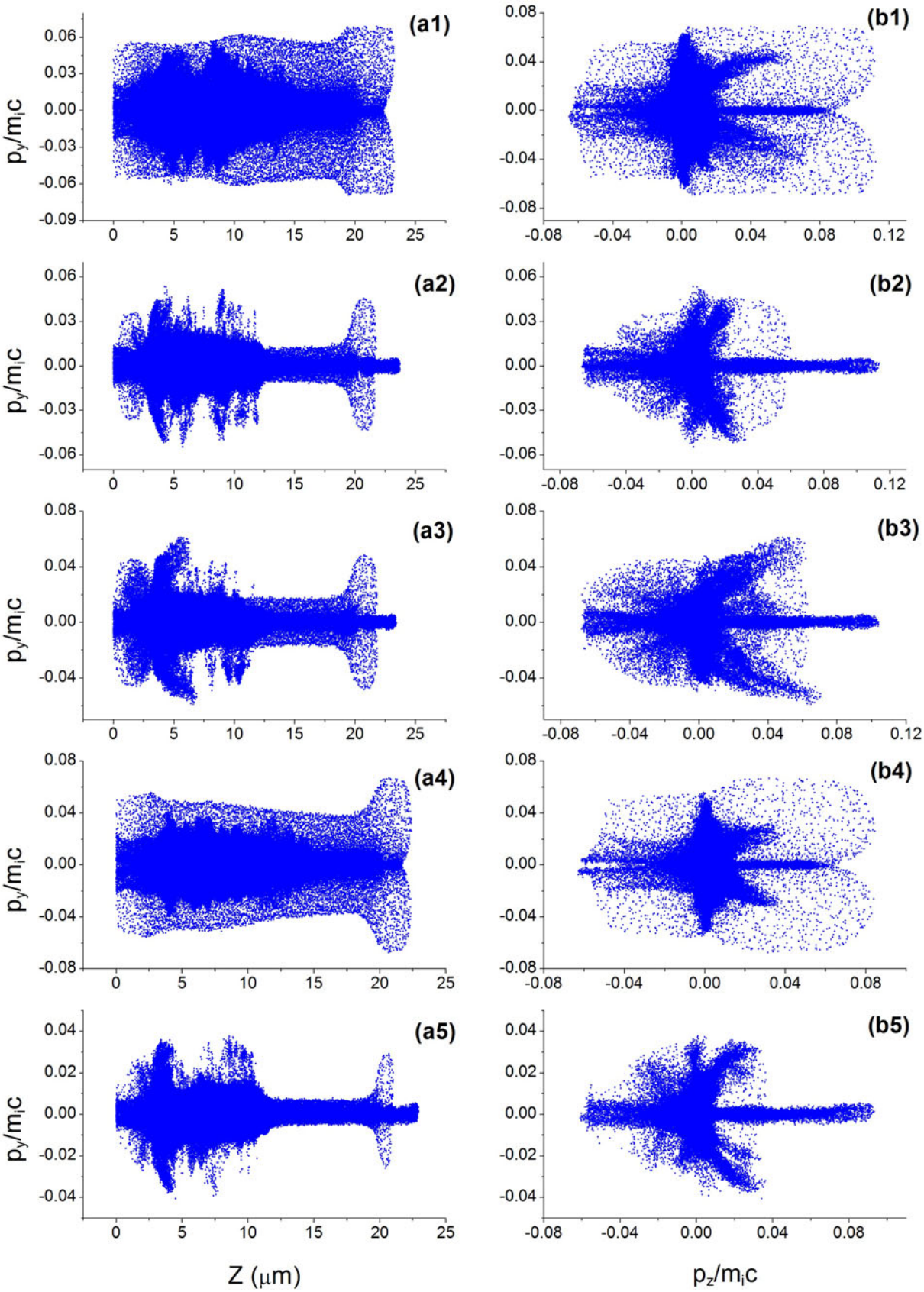

Fig. 5. Normalized proton momentum phase space (a1–a5) p_y/m_ic versus Z (μm) and (b1–b5) p_y/m_ic versus p_z/m_ic at time 147 T_0, respectively, for (a1, b1) CP with $B = 0$ G; (a2, b2) RCP with $B = 50$ MG; (a3, b3) LCP with $B = 50$ MG; (a4, b4) LP with $B = 0$ G; and (a5, b5) LP with $B = 50$ MG.

https://doi.org/10.1017/S0263034618000307 Published online by Cambridge University Press

protons are also observed in these two cases but TNSA overtakes the acceleration process eventually. Since, the ponderomotive force gets enhanced in case of an RCP laser, the electrons gain high energy and move fast across the target rear side which accelerates the protons *via* TNSA mechanism. Thus, front-side acceleration is least and rear-side acceleration is highest in case of an RCP laser in the presence of an axial magnetic field. In case of a LP laser, the protons gain more momentum at the target rear side in the presence of an axial magnetic field as the transverse hot electron motion is restricted due to cyclotron effects resulting more number of hot electrons to flow along the axial direction and generate stronger sheath field which enhances the acceleration as shown in Figure 3(e).

The acceleration of protons at time 147 T_0 is shown in Figure 4. The transverse motion of protons gets considerably reduced in the presence of an axial magnetic field due to cyclotron effects as observed from the proton density plots shown in Figure 4(a1–a5). The protons gain highest forward momentum along the axis at the target rear side in case of an RCP laser as shown in Figure 4(b2). As evident from the proton axial momentum phase space plots, the protons are accelerated mainly *via* TNSA mechanism. It can also be observed from the proton density plots that the laser penetrates deeper into the plasma in the absence of magnetic field. Since, the plasma can expand freely in the absence of magnetic field, the laser penetration does not get affected. The penetration decreases in the presence of magnetic field due to restricted transverse electron motion which causes more number of hot electrons to be present along the axial direction. These hot electrons restrict laser pulse penetration.

A CP laser on propagation through an underdense plasma can generate an axial magnetic field via inverse Faraday effect (Steiger and Woods, 1972; Bychenkov and Tikhonchuk, 1996; Berezhiani *et al.*, 1997; Gorbunov and Ramazashvili, 1998; Naseri *et al.*, 2010). The direction of such magnetic fields in case of an RCP and a LCP laser is opposite to each other (Naseri *et al.*, 2010). These magnetic fields are localized within the laser pulse and do not penetrate in the surrounding plasma. The amplitude is highest along the laser axis and decreases along the transverse directions. These quasistationary magnetic fields are generated in a short time scale $\Delta t = r_0^2/c^2\tau$ (Bychenkov and Tikhonchuk, 1996) where r_0 is the radius of the laser pulse. For the present simulation parameters, we have $\Delta t \approx 0.5$ fs which is a very short time scale as compared with the acceleration time 147 T_0 which corresponds to ≈ 0.5 ps. Hence, the effect caused by these quasistatic short-scale magnetic fields on the acceleration process would be negligible as compared with that caused by the static magnetic field. Moreover, unlike these quasistatic magnetic fields which exist only inside the laser pulse, the applied static magnetic field is present throughout the plasma which is essential for proper guiding of the hot electrons along the laser axis towards the target rear surface.

The axial and transverse momentum phase space plots for all the cases are shown in Figure 5. It can be observed that the axial magnetic field significantly reduces the transverse momentum of the accelerated protons. The protons gain more momentum along the laser axis in the presence of an axial magnetic field which also causes an increase in the collimation of energetic protons. As the sheath electric field is built up at the target rear side and the protons start getting accelerated, they gain momentum both along the transverse and axial directions. This causes the transverse proton momentum to rise suddenly at the target rear side in all the cases which causes the formation of

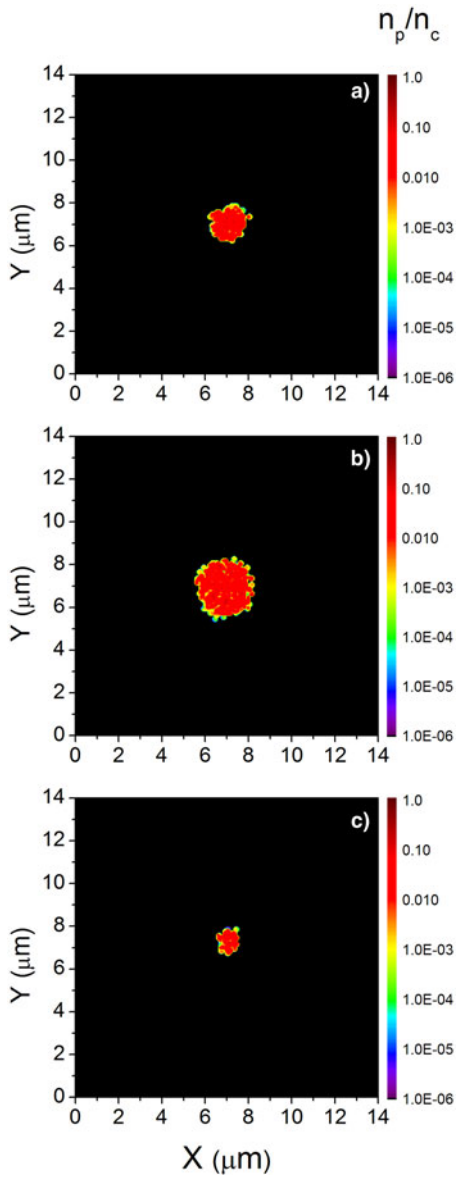

Fig. 6. Proton density distribution in the *XY* plane ($Z = 23.6$ μm) for (a) RCP with $B = 50$ MG at time 147 T_0, (b) LCP with $B = 50$ MG at time 150 T_0, and (c) LP with $B = 50$ MG at time 154 T_0. The proton density n_p is normalized by the critical density $n_c = 1.12 \times 10^{21}$ cm^{-3}.

wing-shaped patterns in the phase space as shown in Figure 5(a1–a5). Since the transverse proton motion throughout the target is significantly reduced in the presence of magnetic field, the transverse momentum seem to rise sharply at the target rear side in this case. This rise in transverse proton momentum experiences a sharp fall making the wing-shaped patterns more prominent and the protons emerge out as a highly collimated beam from the target rear side with remarkably reduced values of transverse momentum. Collimation of protons accelerated by a LP laser in the presence of magnetic field appears to be highest due to smallest spot size among all the cases as shown in Figure 6. However, the axial momentum is observed to be higher in case of an RCP laser as can be concluded by comparing Figure 5(b2) and 5(b5). Moreover, the energy spectrum plotted in Figure 7 shows that the protons accelerated by a LP laser though more collimated but are less energetic than those accelerated by an RCP laser in the presence of magnetic field. In case of a LCP laser, the proton

https://doi.org/10.1017/S0263034618000307 Published online by Cambridge University Press

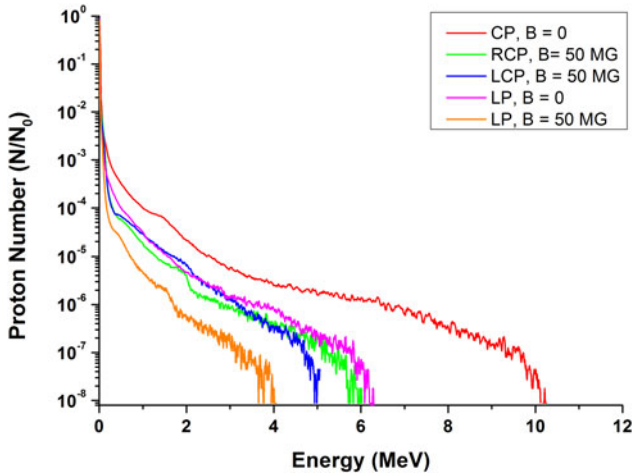

Fig. 7. Proton energy spectrum for CP with $B = 0$ G (red solid), RCP with $B = 50$ MG (green solid), LCP with $B = 50$ MG (blue solid), LP with $B = 0$ G (pink solid), and LP with $B = 50$ MG (orange solid) at time 147 T_0. The proton number N is normalized by the total number of protons N_0 in each case.

beams seem to be collimated but the number of protons having transverse momentum is also high as shown in Figure 5(b3). Hence, collimation in case of a LCP laser is not as effective as compared with that of an RCP laser. Moreover, the maximum proton energy obtained in case of a LCP laser is also lower than that of an RCP laser. Since in the absence of magnetic field, the plasma does not experience any restriction in expansion along transverse directions, it becomes possible for the laser pulse to penetrate deeper and generate more number of energetic protons having higher values of transverse momentum. As the transverse motion of protons is restricted in the presence of magnetic field, the number of protons having transverse momentum values is low. Since, the transverse momentum contributes significantly towards increasing the total energy of protons, the maximum proton energy is less in the presence of magnetic field. The proton energy is thus observed to be highest in case of a CP laser in the absence of magnetic field. The presence of magnetic field thus improves the beam collimation but in turn reduces the maximum energy.

The effect of an axial static magnetic field was also studied by Kuri *et al.* (2017), where the simulations were done for a comparatively dense target and it was observed that both RPA and TNSA were the actively participating mechanisms in the acceleration process. The axial magnetic field causes a synergy in these two processes which can be controlled by either using an RCP or a LCP laser. It was observed that RCP favors TNSA and LCP favors RPA. However, RPA was observed to be the dominating acceleration mechanism in case of dense targets. A minor enhancement of collimation was also observed. In the present work, since the plasma is near-critical, the laser is able to penetrate longer distance inside the plasma and TNSA is the dominating acceleration mechanism. Thus, the cyclotron effects are carried by the laser pulse itself deeper into the plasma which is responsible for the collimation. In case of a dense target as shown by Kuri *et al.* (2017), the cyclotron effects are carried on by the laser pulse up to the hole-boring depth. Beyond this depth, the cyclotron effects are carried forward into the upstream region by the hot electrons generated at the target front surface. Hence, though a significant enhancement in the proton energy was observed, the collimation as speculated from the proton beam spot size was not significant as such.

Creation of a strong magnetic field of the order of 50 MG might seem to be difficult *via* conventional techniques. However, it is to be noted that the maximum proton energy in our simulations is obtained at a time ≈0.5 ps. Thus, instead of having a constant source of magnetic field, production of a high-amplitude static magnetic field sustainable at least up to a time duration of ≈0.5 ps should serve the purpose of collimation as shown in our simulations.

Conclusion

The effect of an axial magnetic field on enhancing the collimation of the energetic proton beams generated from a near-critical plasma target has been investigated with the help of 3D-PIC simulations. The effect of laser pulse polarization combined with the cyclotron effects has also been studied by using both LP and CP laser pulses. The conclusions drawn from the above discussions can be summarized as follows:

(i) Protons are observed to get accelerated *via* TNSA mechanism and the acceleration is higher in case of a CP laser than that of a LP laser.
(ii) Presence of an axial magnetic field reduces the transverse motion of protons and enhances the axial momentum due to cyclotron effects.
(iii) Traces of RPA protons are also observed in case of a CP laser in the absence of magnetic field and LCP laser in the presence of magnetic field. However, TNSA appears to be enhanced in case of an RCP laser in the presence of magnetic field.
(iv) In case of a LP laser, the presence of an axial magnetic field increases the acceleration as the transverse hot electron motion is reduced due to cyclotron effects and the hot electron flow across the rear side along the axis is increased resulting stronger sheath formation and hence enhanced acceleration.
(v) Presence of an axial magnetic field significantly enhances the collimation of proton beams. Collimation appears to be highest in case of a LP laser in the presence of magnetic field due to its smallest spot size. However, proton axial momentum is observed to be highest with good collimation in case of an RCP laser in the presence of magnetic field.
(vi) When the acceleration process starts, transverse proton momentum rises sharply at the target rear side. In the presence of magnetic field, the transverse momentum after rising falls sharply due to cyclotron effects and the proton beams emerge out into the vacuum with very low values of transverse momentum and are therefore highly collimated.
(vii) It is observed that though the presence of magnetic field enhances collimation, it in turn reduces maximum proton energy. This might be due to reduction in transverse momentum which has a significant contribution in the total proton energy.

Acknowledgments. The authors are thankful to the Board of Research in Nuclear Sciences (BRNS), Department of Atomic Energy (DAE), Government of India for providing us the financial support *via* Project No. 2012/34/61/BRNS.

References

Berezhiani VI, Mahajan SM and Shatashvili NL (1997) Theory of magnetic field generation by relativistically strong laser radiation. *Physical Review E* **55**, 995.

https://doi.org/10.1017/S0263034618000307 Published online by Cambridge University Press

Bin JH, Ma WJ, Wang HY, Streeter MJV, Kreuzer C, Kiefer D, Yeung M, Cousens S, Foster PS, Dromey B, Yan XQ, Ramis R, Meyer-ter-Vehn J, Zepf M and Schreiber J (2015) Ion acceleration using relativistic pulse shaping in near-critical-density plasmas. *Physical Review Letters* **115**, 064801.

Borghesi M, Schiavi A, Campbell DH, Haines MG, Willi O, Mackinnon AJ, Patel P, Galimberti M and Gizzi LA (2003) Proton imaging detection of transient electromagnetic fields in laser-plasma interactions. *Review of Scientific Instruments* **74**, 1688.

Borhanian J, Kourakis I and Sobhanian S (2009) Electromagnetic envelope solitons in magnetized plasma. *Physics Letters A* **373**, 3667.

Bulanov SV and Esirkepov TZ (2007) Comment on "collimated multi-MeV ion beams from high-intensity laser interactions with underdense plasma". *Physical Review Letters* **98**, 049503.

Bulanov SV, Esirkepov TZ, Khoroshkov VS, Kuznetsov AV and Pegoraro F (2002) Oncological hadrontherapy with laser ion accelerators. *Physics Letters A* **299**, 240.

Bulanov SS, Bychenkov VY, Chvykov V, Kalinchenko G, Litzenberg DW, Matsuoka T, Thomas AGR, Willingale L, Yanovsky V, Krushelnick K and Maksimchuk A (2010) Generation of GeV protons from 1 PW laser interaction with near critical density targets. *Physics of Plasmas* **17**, 043105.

Bulanov SV, Esirkepov TZ, Kando M, Koga JK, Hosokai T, Zhidkov AG and Kodama R (2013) Nonlinear plasma wave in magnetized plasmas. *Physics of Plasmas* **20**, 083113.

Bychenkov VY and Tikhonchuk VT (1996) Magnetic field generation by short ultraintense laser pulse in underdense plasmas. *Laser and Particle Beams* **14**, 55.

Bychenkov VY, Tikhonchuk VT and Tolokonnikov SVJ (1999) Nuclear reactions triggered by laser-accelerated high-energy ions. *Journal of Experimental and Theoretical Physics* **88**, 1137.

Clark EL, Krushelnick K, Davies JR, Zepf M, Tatarakis M, Beg FN, Machacek A, Norreys PA, Santala MIK, Watts I and Dangor AE (2000) Measurements of energetic proton transport through magnetized plasma from intense laser interactions with solids. *Physical Review Letters* **84**, 670.

Debray F and Frings P (2013) State of the art and developments of high field magnets at the "Laboratoire National des Champs Magnétiques Intenses". *Comptes Rendus Physique* **14**, 2.

Farina D, Lontano M and Bulanov S (2000) Relativistic solitons in magnetized plasmas. *Physical Review E* **62**, 4146.

Fuchs J, Antici P, d'Humieres E, Lefebvre E, Borghesi M, Brambrink E, Cecchetti CA, Kaluza M, Malka V, Manclossi M, Meyroneinc S, Mora P, Schreiber J, Toncian T, Pepin H and Audebert P (2006) Laser-driven proton scaling laws and new paths towards energy increase. *Nature Physics* **2**, 48.

Fujioka S, Zhang Z, Ishihara K, Shigemori K, Hironaka Y, Johzaki T, Sunahara A, Yamamoto N, Nakashima H, Watanabe T, Shiraga H, Nishimura H and Azechi H (2013) Kilotesla magnetic field due to a capacitor-coil target driven by high power laser. *Scientific Reports* **3**, 1170.

Fukuda Y, Faenov AY, Tampo M, Pikuz TA, Nakamura T, Kando M, Hayashi Y, Yogo A, Sakaki H, Kameshima T, Pirozhkov AS, Ogura K, Mori M, Esirkepov TZ, Koga J, Boldarev AS, Gasilov VA, Magunov AI, Yamauchi T, Kodama R, Bolton PR, Kato Y, Tajima T, Daido H and Bulanov SV (2009) Energy increase in multi-MeV ion acceleration in the interaction of a short pulse laser with a cluster-gas target. *Physical Review Letters* **103**, 165002.

Gong JX, Cao LH, Pan KQ, Xiao KD, Wu D, Zheng CY, Liu ZJ and He XT (2017) Enhancement of proton acceleration by a right-handed circularly polarized laser interaction with a cone target exposed to a longitudinal magnetic field. *Physics of Plasmas* **24**, 053109.

Gorbunov LM and Ramazashvili RR (1998) Magnetic field generated in a plasma by a short, circularly polarized laser pulse. *Journal of Experimental and Theoretical Physics* **87**, 461.

Hosokai T, Kenishita K, Zhidkov A, Maekawa A, Yamazaki A and Uesaka M (2006) Effect of external static magnetic field on the emittance and total charge of electron beams generated by laser-wakefield acceleration. *Physical Review Letters* **97**, 075004.

Khoroshkov VS and Minakova EI (1998) Proton beams in radiotherapy. *European Journal of Physics* **19**, 523.

King NSP, Ables E, Adams K, Alrick KR, Amann JF, Balzar S, Barnes PD, Crow ML, Cushing SB, Eddleman JC, Fife TT, Flores P, Fujino D, Gallegos RA, Gray NT, Hartouni EP, Hogan GE, Holmes VH, Jaramillo SA, Knudsson JN, London RK, Lopez RR, McDonald TE, McClelland JB, Merrill FE, Morley KB, Morris CL, Naivar FJ, Parker EL, Park HS, Pazuchanics PD, Pillai C, Riedel CM, Sarracino JS, Shelley FE, Stacy HL, Takala BE, Thompson R, Tucker HE, Yates GJ, Ziock H-J and Zumbro JD (1999) An 800-MeV proton radiography facility for dynamic experiments. *Nuclear Instruments & Methods in Physics Research, Section A* **424**, 84.

Krushelnick K, Clark EL, Najmudin Z, Salvati M, Santala MIK, Tatarakis M, Dangor AE, Malka V, Neely D, Allott R and Danson C (1999) Multi-MeV ion production from high-intensity laser interactions with underdense plasmas. *Physical Review Letters* **83**, 737.

Kuri DK, Das N and Patel K (2017) Proton acceleration from magnetized overdense plasmas. *Physics of Plasmas* **24**, 013112.

Maksimchuk A, Gu S, Flippo K, Umstadter D and Bychenkov VY (2000) Forward ion acceleration in thin films driven by a high-intensity laser. *Physical Review Letters* **84**, 4108.

Mondal S, Narayanan V, Ding WJ, Lad AD, Hao B, Ahmad S, Wang WM, Sheng ZM, Sengupta S, Kaw P, Das A and Kumar GR (2012) Direct observation of turbulent magnetic fields in hot, dense laser produced plasmas. *Proceedings of the National Academy of Sciences of the USA* **109**, 8011.

Mora P (2003) Plasma expansion into a vacuum. *Physical Review Letters* **90**, 185002.

Nakamura T, Bulanov SV, Esirkepov TZ and Kando M (2010a) High-energy ions from near-critical density plasmas via magnetic vortex acceleration. *Physical Review Letters* **105**, 135002.

Nakamura T, Tampo M, Kodama R, Bulanov SV and Kando M (2010b) Interaction of high contrast laser pulse with foam-attached target. *Physics of Plasmas* **17**, 113107.

Naseri N, Bychenkov VY and Rozmus W (2010) Axial magnetic field generation by intense circularly polarized laser pulses in underdense plasmas. *Physics of Plasmas* **17**, 083109.

Naumova N, Schlegel T, Tikhonchuck VT, Labaune C, Sokolov IV and Mourou G (2009) Hole boring in a DT pellet and fast-ion ignition with ultraintense laser pulses. *Physical Review Letters* **102**, 025002.

Remington BA, Drake RP and Takabe H (2000) A review of astrophysics experiments on intense lasers. *Physics of Plasmas* **7**, 1641.

Roth M, Cowan TE, Key MH, Hatchett SP, Brown C, Fountain W, Johnson J, Pennington DM, Snavely RA, Wilks SC, Yasuike K, Ruhl H, Pegoraro F, Bulanov SV, Campbell EM, Perry MD and Powell H (2001) Fast ignition by intense laser-accelerated proton beams. *Physical Review Letters* **86**, 436.

Sandhu AS, Dharmadhikari AK, Rajeev PP, Kumar GR, Sengupta S, Das A and Kaw PK (2002) Laser-generated ultrashort multimegagauss magnetic pulses in plasmas. *Physical Review Letters* **89**, 225002.

Santos JJ, Bailly-Grandvaux M, Giuffrida L, Forestier-Colleoni P, Fujioka S, Zhang Z, Korneev P, Bouillaud R, Dorard S, Batani D, Chevrot M, Cross JE, Crowston R, Dubois J-L, Gazave J, Gregori G, d'Humieres E, Hulin S, Ishihara K, Kojima S, Loyez E, Marques J-R, Morace A, Nicolai P, Peyrusse O, Poye A, Raffestin D, Ribolzi J, Roth M, Schaumann G, Serres F, Tikhonchuk VT, Vacar P and Woolsey N (2015) Laser-driven platform for generation and characterization of strong quasi-static magnetic fields. *New Journal of Physics* **17**, 083051.

Sarkisov GS, Bychenkov VY, Novikov VN, Tikhonchuk VT, Maksimchuk A, Chen S-Y, Wagner R, Mourou G and Umstadter D (1999) Self-focusing, channel formation, and high-energy ion generation in interaction of an intense short laser pulse with a He jet. *Physical Review E* **59**, 7042.

Schlegel T, Naumova N, Tikhonchuck VT, Labaune C, Sokolov IV and Mourou G (2009) Relativistic laser piston model: ponderomotive ion acceleration in dense plasmas using ultraintense laser pulses. *Physics of Plasmas* **16**, 083103.

Schmit PF, Knapp PF, Hansen SB, Gomez MR, Hahn KD, Sinars DB, Peterson KJ, Slutz SA, Sefkow AB, Awe TJ, Harding E, Jennings CA, Chandler GA, Cooper GW, Cuneo ME, Geissel M, Harvey-Thompson AJ, Herrmann MC, Hess MH, Johns O, Lamppa DC, Martin MR, McBride RD, Porter JL, Robertson GK, Rochau GA,

https://doi.org/10.1017/S0263034618000307 Published online by Cambridge University Press

Rovang DC, Ruiz CL, Savage ME, Smith IC, Stygar WA and Vesey RA (2014) Understanding fuel magnetization and mix using secondary nuclear reactions in magneto-inertial fusion. *Physical Review Letters* **113**, 155004.

Sharma A, Liu CS and Tripathi VK (2010) Cyclotron effects on double layer ion acceleration from laser-irradiated thin foils. *Physics of Plasmas* **17**, 013101.

Sims JR, Rickel DG, Swenson CA, Schillig JB and Ammerman CN (2008) Assembly, commissioning and operation of the NHMFL 100 Tesla multi-pulse magnet system. *IEEE Transactions on Applied Superconductivity* **18**, 587.

Snavely RA, Key MH, Hatchett SP, Cowan TE, Roth M, Phillips TW, Stoyer MA, Henry EA, Sangster TC, Singh MS, Wilks SC, MacKinnon A, Offenberger A, Pennington DM, Yasuike K, Langdon AB, Lasinski BF, Johnson J, Perry MD and Campbell EM (2000) Intense high-energy proton beams from petawatt-laser irradiation of solids. *Physical Review Letters* **85**, 2945.

Steiger AD and Woods CH (1972) Intensity-dependent propagation characteristics of circularly polarized high-power laser radiation in a dense electron plasma. *Physical Review A* **5**, 1467.

Tatarakis M, Watts I, Beg FN, Clark EL, Dangor AE, Gopal A, Haines MG, Norreys PA, Wagner U, Wei M-S, Zepf M and Krushelnick K (2002) Laser technology: measuring huge magnetic fields. *Nature* **415**, 280.

Upadhyay A, Patel K, Rao BS, Naik PA and Gupta PD (2012) Three-dimensional simulation of laser–plasma-based electron acceleration. *Pramana, Journal of Physics* **78**, 613.

Wang WM, Gibbon P, Sheng ZM and Li YT (2015) Magnetically assisted fast ignition. *Physical Review Letters* **114**, 015001.

Wei MS, Mangles SPD, Najmudin Z, Walton B, Gopal A, Tatarakis M, Dangor AE, Clark EL, Evans RG, Fritzler S, Clarke RJ, Hernandez-Gomez C, Neely D, Mori W, Tzoufras M and Krushelnick K (2004) Ion acceleration by collisionless shocks in high-intensity-laser–underdense-plasma interaction. *Physical Review Letters* **93**, 155003.

Wilks SC, Kruer WL, Tabak M and Langdon AB (1992) Absorption of ultra-intense laser pulses. *Physical Review Letters* **69**, 1383.

Wilks SC, Langdon AB, Cowan TE, Roth M, Singh M, Hatchett S, Key MH, Pennington D, MacKinnon A and Snavely RA (2001) Energetic proton generation in ultra-intense laser–solid interactions. *Physics of Plasmas* **8**, 542.

Willingale L, Mangles SPD, Nilson PM, Clarke RJ, Dangor AE, Kaluza MC, Karsch S, Lancaster KL, Mori WB, Najmudin Z, Schreiber J, Thomas AGR, Wei MS and Krushelnick K (2006) Collimated multi-MeV ion beams from high-intensity laser interactions with underdense plasma. *Physical Review Letters* **96**, 245002.

Willingale L, Nagel SR, Thomas AGR, Bellei C, Clarke RJ, Dangor AE, Heathcote R, Kaluza MC, Kamperidis C, Kneip S, Krushelnick K, Lopes N, Mangles SPD, Nazarov W, Nilson PM and Najmudin Z (2009) Characterization of high-intensity laser propagation in the relativistic transparent regime through measurements of energetic proton beams. *Physical Review Letters* **102**, 125002.

Wilson TC, Li FY, Weikum M and Sheng ZM (2017) Influence of strong magnetic fields on laser pulse propagation in underdense plasma. *Plasma Physics and Controlled Fusion* **59**, 065002.

Yang XH, Yu W, Xu H, Yu MY, Ge ZY, Xu BB, Zhuo HB, Ma YY, Shao FQ and Borghesi M (2015) Propagation of intense laser pulses in strongly magnetized plasmas. *Applied Physics Letters* **106**, 224103.

https://doi.org/10.1017/S0263034618000307 Published online by Cambridge University Press